Millimetre – wave insect vision sensors for collision avoidance in space

David C. Goodfellow*[a] and Derek Abbott[a]

[a]Centre for Biomedical Engineering (CBME) and
Centre for High Performance Integrated Technologies and Systems (CHiPTec),
Department of Electrical and Electronic Engineering, The University of Adelaide,
SA 5005, Adelaide, Australia.

ABSTRACT

A novel collision avoidance sensor with possible application in satellite navigation is presented. Passive radiometric detection of colliding objects is used, offering the advantage that it does not interfere with satellite communication or guidance systems. Operation in the millimetre-wave band allows the possibility of full scale integration of front-end detection circuitry with the back-end signal processing. And the use of insect vision models, in the processing, leads to reduced circuit complexity.

Such a compact sensing system could be ideal for integration into the structure of nanosatellites[1] – these are very small satellites weighing less than 10 kg. These next generation satellites will operate in clusters, thus detection and avoidance of neighbouring satellites is vital to the success of such configurations.

This paper discusses the design and structure of our mm-wave collision avoidance sensor[2] and predicts the performance[3] for the orbital environment. The effects of strong radiation sources and the dynamics of satellite heating and motion are explored. Methods and techniques for obtaining this information are discussed.

Keywords: mm-Wave sensors, Collision avoidance, Radiometry, Nanosatellites, Integrated antenna arrays

1. INTRODUCTION

The use of a novel millimetre-wave insect vision motion sensor for nanosatellite collision avoidance is investigated. It appears that the possible implementation of these nanosatellites[1,4–6] is for them to function in large clusters. *Collective behaviour* within these clusters similar to that of an insect colony could be used for purposes of regrouping and adapting the effective communication aperture. This leads to the requirement for advanced on-board guidance systems. These systems will need to include sensors for collision avoidance. In accordance with low interference in communications or telemetric circuitry, these sensors should passively detect the motion of neighbouring satellites. Radiometric sensors can be employed for this purpose in much the same way as they are used on satellites now for the remote sensing of the Earth's atmosphere and surface.[3,7–10]

A sensor of this type operating in the millimetre-wave band[11] of the electromagnetic spectrum (30 – 300 GHz) provides a very compact, low weight, and inexpensive sensor. A planar structure will allow conformity with the small size of a nanosatellite structure. The use of a fully integrated sensor with primary applications in automobile collision avoidance[2,12] is investigated for this possible application. Other applications for the hardware include, collision avoidance and warning systems for landing and taxiing aircraft, close range all-weather object detection for ship docking and in-port navigation, industrial monitoring of hazardous manufacturing processes, as well as military missile seekers and synthetic vision for ground vehicles. System design and considerations for nanosatellite integration are discussed.

*Correspondence: E-mail: dcgoodfe@eleceng.adelaide.edu.au; Telephone: 61 8 8303 3403; Fax: 61 8 8303 4360

Part of the SPIE Conference on Mobile Robots XIV
Boston, Massachusetts • September 1999
SPIE Vol. 3838 • 0277-786X/99/$10.00

2. COLLISION AVOIDANCE SENSOR

The radiometric system under investigation employs a beamforming lens which allows simultaneous scanning through a linear antenna array over a large field of view. The advantages of using this technology are the inherent wide bandwidth of the lens due to a frequency independent structure, the possibility of full scale monolithic integration with detection circuitry at high mm-wave frequencies and the ability to employ insect vision motion detection algorithms through input/output channel discrimination. Advantage can also be taken of the reduction of the quality of the image processing needed for detection, which reduces the otherwise high cost of operating in this frequency band. It is possible to design the motion sensor without the need for many active components in the circuitry of the detector stage, since insect vision motion detection requires less sensitivity than imaging, making the system simpler, less expensive, more compact and easier to fabricate. The front-end system topology for operation at 37 GHz using microstrip integrated circuit technologies at mm-wavelengths (MMIC) was presented in Goodfellow *et. al.*[2] and is briefly described here for higher frequencies.

2.1. Structure

The linear antenna array for use at a planar single chip level is a 10 element half-wavelength folded dipole antenna array, allowing five beams through a Rotman lens beamformer.[2,13] At 94 GHz the front-end microstrip system has an aperture width of 22 mm and an approximate total length of 35mm incorporating feed lengths and based on an $F/D = 1$ (lens focal length to aperture width ratio) design. A schematic of the system is shown in Fig. 1. The aperture width includes an antenna element separation of a half-wavelength, to avoid mutual coupling and grating lobes in the radiation pattern*. The elements are matched to the feed lines via *baluns* (balanced to unbalanced transformers) to reduce reflection losses.

The microstrip Rotman lens is a parallel–plate region with beam ports and array ports distributed along opposite contours, as shown in Fig. 1. By virtue of the design, a central beam port can provide equal path lengths to each array element. An off–set beam port (off–axis) will produce a path length and hence a phase gradient along the array giving a steered beam. With an equispaced array, a perfectly linear phase gradient along the array is realised for three beam directions, where beam ports are located at the three perfect focal points on the beam port contour.

To realise a full MMIC design the system uses microstrip elements. That is, microstrip antenna elements with microstrip transmission lines feeding flared microstrip array ports of the lens for impedance matching and better coupling form essentially a rectangular-to-parallel–plate waveguide region (Fig. 1). The lens size must take into account the substrate used to construct the lens, where it is reduced by the square root of the relative permittivity of the substrate ϵ_r. The plate separation of the lens is made less than half the wavelength inside the substrate ($\lambda_d/2$) to avoid any twisting of the TEM mode propagating in the parallel–plate region.

The level of performance of the antenna array, feeds and lens is governed by the losses associated with the materials and structure. The effects of these are now discussed.

2.2. Performance

The losses through the system derive from the microstrip losses into the substrate media through surface wave propagation[15]; the input feed microstrip-to-lens medium transition; lens losses due to spill-over and abberations[2,13,16]; the lens-to-microstrip output feeds; and losses in the detection stage on chip (amplification and mixers for downconversion to IF etc). The theoretical radiation pattern of this system is shown in Fig. 2, showing a scan coverage of $\pm 26°$ for beams of 5° beamwidth and sidelobe levels of -16 dB. These values can be changed through modifications to the antenna and lens designs. More beams will obviously give a greater scan width, yet as you place beam ports closer to the edges of the lens contours the level of spill-over increases, reducing the performance of these outside ports. Importantly the sidelobes are to be kept as low as possible so as to maintain good main beam efficiency and to decrease radiometric contributions from neighbouring sources. This effect is explored later. Many trade-offs exist in the Rotman lens design due to the large number of degrees of freedom.

These include: off-axis focal point angle (governing scan width and contour shape); focal lengths (governing F/D ratio); beam port number and placement (controlling number of beams and level of spill-over power); and beam and array port feed orientation (most conveniently taken as pointing to the centre of the opposite contour). A further

*Actually Gagnon[14] showed that the grating lobes only appear in the lens space and not in the scan space, yet this will still effect antenna gain at wide scan angles.

degree of freedom in the lens design is achieved if we make the internal lens angle θ not equal to the external beam angle ψ, as assumed by Rotman *et. al.*.[13] This produces a parameter called the beam to ray angle ratio, given by

$$\beta = \frac{\sin\psi}{\sin\theta}. \tag{1}$$

We can then gain control over design parameters such as the array port spacing ($\beta \times$ array element spacing) near the centre of the array port contour.

One of the most important losses to minimise are those of spill-over. This can be done by redesigning the sidewall structure, using dummy ports or including dielectric absorber. By extending the sidewalls into a 'batman' configuration,[12] the winged sections in Fig. 1, the spill–over energy is confined within these regions where it can be dissipatively extracted. This configuration more completely confines the spill–over energy than the simple triangular configuration employed by Rausch *et. al.*,[17] yet, certain aspects of this design need to be carefully considered. The taper of the inlets into the side wings need to be constructed correctly so that energy from all possible incidence angles pass through the inlets.

Through appropriate design these losses can be kept to a minimum. The levels of these losses allowable for radiometric detection are now explored.

2.3. Sensitivity

A radiometer takes the output power of the antenna over a particular bandwidth B and can amplify this by an amount G before presenting it in a suitable fashion to the detector. For a direct detection radiometer the output is just the power received, given by

$$P = k\,B\,G\,(T_A + T_N), \tag{2}$$

where k is Boltzmann's constant, $G = 1$, and T_A and T_N are the antenna temperature and noise temperature of the system, respectively. The sensitivity relies on the antenna temperature, the noise temperature, the bandwidth and the integration time τ of the detector in the following way

$$\Delta T = \frac{T_A + T_N}{\sqrt{B\,\tau}}. \tag{3}$$

Skou[3] quotes typical values for these: an antenna temperature of say 200 K; a noise temperature of 800 K; a bandwidth of 100 MHz; and an integration time of 10 ms, which lead to a sensitivity (or standard deviation of output signal) of $\Delta T = 1$ K.

Apart from sensitivity, another important factor is the absolute accuracy of the system. That is, losses in the radiometer feeds can cause a slight change in the measured temperature value. It can be shown that this difference T_D is given by

$$T_D = \ell\,(T_0 - T_1), \tag{4}$$

where T_0 and T_1 are the physical and input temperatures of the feed, respectively and ℓ is the loss of the feed. For a well designed feed system these losses are small, but even for losses as small as 0.01 dB with $T_0 = 300$ K and $T_1 = 100$ K, the difference, T_D is 0.5 K. This loss corresponds to a reflection coefficient of -26 dB, thus it is important to maintain a reflection coefficient better than this value.[3]

The importance of the absolute accuracy and sensitivity of the system depends greatly on the signal levels being detected. If the background radiometric temperature levels are close to the temperature levels of the satellite structures strict tolerances in the temperature resolution of the system will have to be applied. The temperatures expected must be investigated to determine these tolerances.

These effects must be considered when designing the feed system. This design is now discussed.

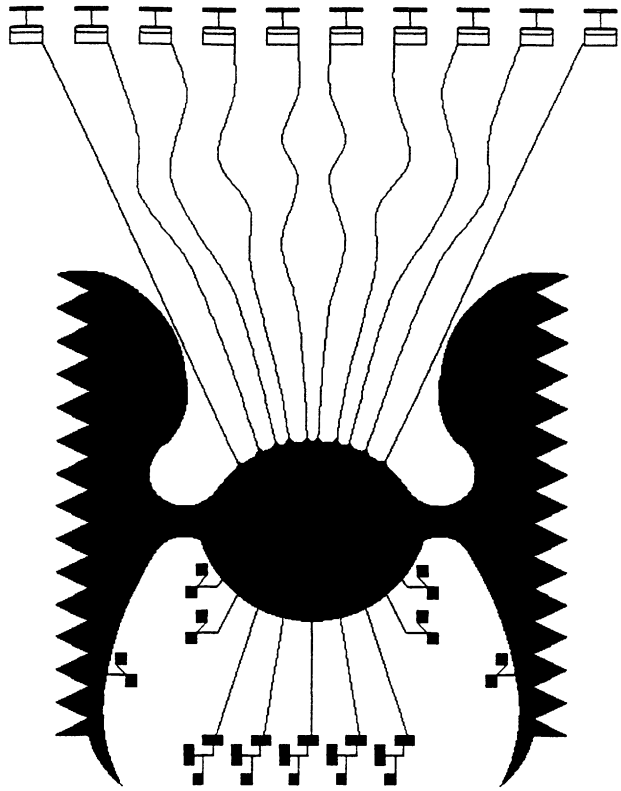

Figure 1. Schematic of 5 beam microstrip Rotman lens system showing 10 element folded dipole array with matching circuitry, microstrip feeds to array and beam ports, dummy ports with dissipative loads and output circuitry.

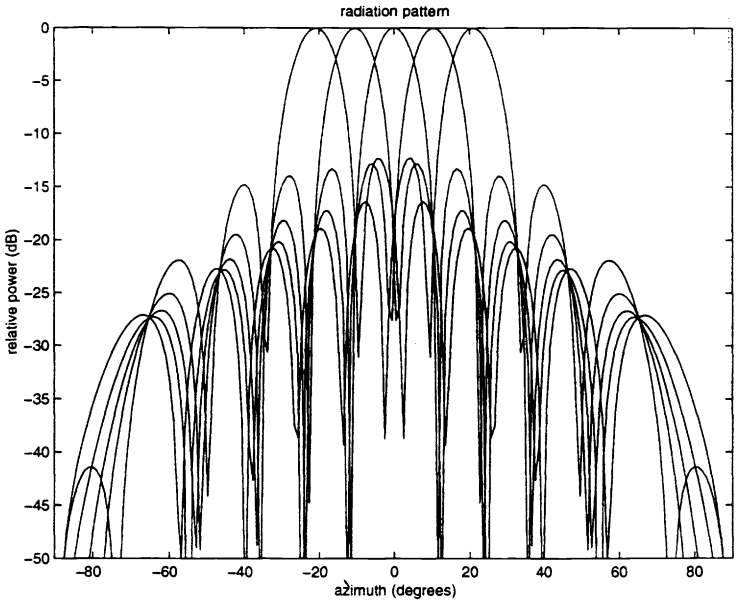

Figure 2. Calculated radiation pattern for 5 beam Rotman lens.

3. SATELLITE RADIOMETRY

At higher frequencies, > 90 GHz, full scale integration is possible due to the smaller resultant geometries. That is, the motion detection system can be completely fabricated onto a single chip if a linear antenna array is used. Several of these sensors can be distributed across the surfaces of a nanosatellite allowing complete coverage of the immediate scene. For radiometric collision avoidance the fundamental consideration is the ability of the sensor to discern the signals of incoming colliding objects from the background. In order to ascertain whether or not a satellite fitted with a radiometric motion sensor could successfully detect another satellite the *brightness temperature* [3] of that satellite needs to be calculated and compared to the brightness temperatures of the Sun, Earth and the cosmic background radiation.

The most convenient method to obtain these values is to consider their blackbody curves or Planck-law distributions.

3.1. Brightness

The blackbody curve or the Planck's law distribution[18,10] of a body is a useful tool in telling us how that body radiates along the entire electromagnetic spectrum. The distribution measures the *brightness* of the object against either frequency or wavelength. For convenience we chose to look at brightness with wavelength. The brightness of a blackbody radiator in wavelengths is determined by[19]

$$B_\lambda = \frac{2hc^2}{\lambda^5 e^{hc/kT\lambda} - 1}, \tag{5}$$

where λ is the wavelength, h is Planck's constant, 6.63×10^{-34}Js, c is the speed of light, k is again Boltzmann's constant $1.38 \times 10^{-23}\mathrm{J\,K^{-1}}$, and T is the temperature of interest. The methods used to calculate these temperatures are discussed in Goodfellow *et. al.*[20] and are briefly outlined here.

The surface temperature of the Sun can be calculated since we know the value of the solar energy flux[19] S at the top of the Earth's atmosphere is 1.38 $\mathrm{kWm^{-2}}$ and we know the mean Sun–Earth distance, 1.5×10^{11}m. Calculating the total radiated power from the Sun will then yield it's temperature. Assuming that the Sun is a blackbody radiator, this can be done by considering the relationship $P = kAT^4$, where $A = 4\pi R_S^2$ is the surface area of the Sun (and R_S is the radius of the Sun, 7×10^8 m), k is Boltzmann's constant, and T is the surface temperature. Rearranging, yields the Sun's surface temperature $T \approx 5800$ K.

From this the equivalent blackbody temperature of the Earth can be calculated by considering the radiative equilibrium condition, incoming flux = outgoing flux, or $(1-a)S\pi R_E^2 = E4\pi R_E^2$, where a is the planetary *albedo*[†] and R_E is the radius of the Earth. Rearranging and calculating we obtain the Earth's irradiance $E = 241\,\mathrm{W\,m^{-2}}$. The equivalent blackbody temperature of the Earth is gained by assuming that the Earth is radiating as a blackbody and considering the *Stefan–Boltzmann law*, $E = \sigma T^4$. Which leads to $T_E = 255$ K, where T_E is known as the effective temperature of the Earth.

The microwave background radiation[21,22] has a temperature of 2.75 K, and is believed to be the remnants of the *big bang*. The existence of this constant background radiation level in the band that we are interested in could have an effect on any radiometric measurements taken and so it is important to consider this radiation.

The blackbody curves representing the brightness with wavelength values for the Earth, Sun and the cosmic background are shown in Fig. 3, with the mm-wave band shown in bold. Comparison of the brightness values in this region with those of a satellite will provide information about the possibility of detection. Thus, the brightness values for the satellite need to be calculated.

4. SATELLITES

We consider a small perfectly black spherical satellite in orbit around the Earth. To calculate the radiative equilibrium temperature of the satellite in the Earth's shadow we consider the amount of heat imparted to the satellite by the Earth, dQ. This is given by

$$dQ = \pi r^2 L d\Omega, \tag{6}$$

[†]The planetary albedo is the fraction of the total incident solar radiation that is reflected back into space without absorption. The Earth's albedo is 0.30.

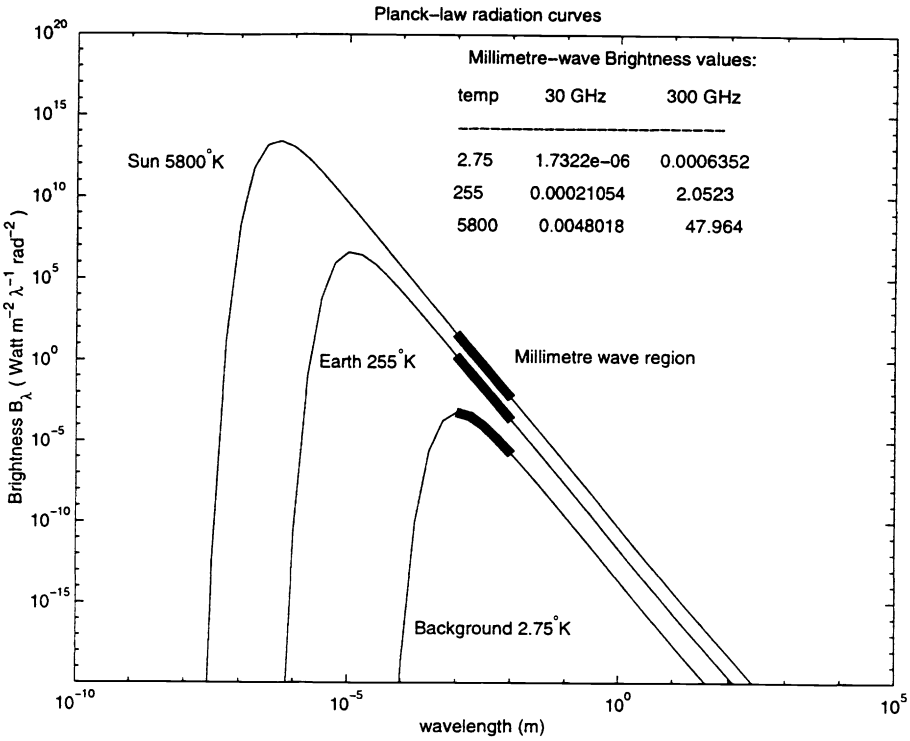

Figure 3. Blackbody brightness vs. temperature curves for earth, the sun and the cosmic background.

where r is the radius of the satellite, L is the radiance of the radiation emitted by the Earth and Ω is the solid angle subtended by the Earth as seen from the satellite. Now $E = \pi L$ for radiation emitted from an infinite plane surface with uniform radiance in all directions. Then integrating over the entire arc of solid angle and equating to $Q = AE$, which also represents the heat, we obtain

$$4\pi r^2 \sigma T_S^4 = \Omega r^2 \sigma T_E^4,$$

which becomes

$$T_S = T_E \Big(\frac{\Omega}{4\pi}\Big)^{1/4}. \tag{7}$$

This temperature is modified when the satellite comes out of the Earth's shadow where it is also heated by the Sun. Thus, Eq.(7) becomes

$$T_S^4 = \frac{1}{4}\Big(\frac{R_{sun}}{D}\Big)^2 T_{sun}^4 + \frac{1}{4}\Big(\frac{\Omega}{\pi}\Big) T_E^4, \tag{8}$$

where D is approximately the Earth–Sun mean distance minus the satellites distance from the Earth. From these temperature values the brightness values of the satellite are now determined. Yet, in order to determine the radiometric signal levels from these brightness values the corresponding *brightness temperatures* need to be calculated.

5. BRIGHTNESS TEMPERATURE

The brightness temperature is related to the brightness in wavelengths by the following

$$T_B = \frac{\lambda^4 B_\lambda}{2ck\Delta\lambda}. \tag{9}$$

For reasons of simplicity we firstly calculate the brightness temperatures for a single frequency such that the bandwidth $\Delta\lambda$ is unity. The radiometer detects this brightness temperature as an increase in antenna temperature T_A, where

$$T_A = \eta T_B, \tag{10}$$

where η is the main antenna beam efficiency, which for a good system is of the order of 95%. Thus, the sidelobe beam efficiency of the radiation pattern is $(1-\eta)$, which is 5% in the above case. The contributions of the main and secondary beams on brightness temperature detection are as follows

$$T_A = \eta T_{ml} + (1-\eta) T_{sl}, \tag{11}$$

where T_{ml} and T_{sl} are the main lobe and sidelobe brightness temperatures respectively.

Therefore, if a satellite passes into the main lobe of a radiometer fitted on another satellite, it's brightness temperature will be detected along with possible sidelobe contributions from the Sun, Earth and cosmic background, such that Eq.(11) becomes

$$T_{Asat} = 0.95 T_{Bsat} + 0.05(T_{Bsun} + T_{Bearth} + T_{Bcb}). \tag{12}$$

Fig. 4 shows the brightness and antenna temperatures calculated for satellites in the Earth's shadow and in full sunlight at various orbit heights from 400 km (LEO) to 2000 km using Eq.(12). As expected the effect of the Earth and background brightness temperatures on the eclipsed satellite antenna temperature is small. The extra contribution from the Sun's brightness temperature almost doubles the antenna temperature, displaying the effect of solar heating.

For a complete analysis it is important therefore to track the satellite temperature through a complete orbit of approximately 92 minutes. This analysis was carried out by Müncheberg *et. al.* for 10 kg aluminium nanosatellites with cubic dimensions of 5, 7.5, 10, 12.5 and 15 cm and heat capacity of 880 $\mathrm{J\,kg^{-1}\,K^{-1}}$ at 400 km orbits, the results shown in Fig. 3 of Müncheberg *et. al.*[1] The maximum and minimum equilibrium temperatures are equivalent for different sized satellites, since the amount of absorbed and then re-radiated energy is proportional to the surface area of the satellite. Müncheberg *et. al.* showed that the satellite temperature never reached the equilibrium limits through the orbit, rather they ranged between the two. Basically not enough time elapsed in either eclipsed or full sun regions such that the satellite could sufficiently heat or cool.

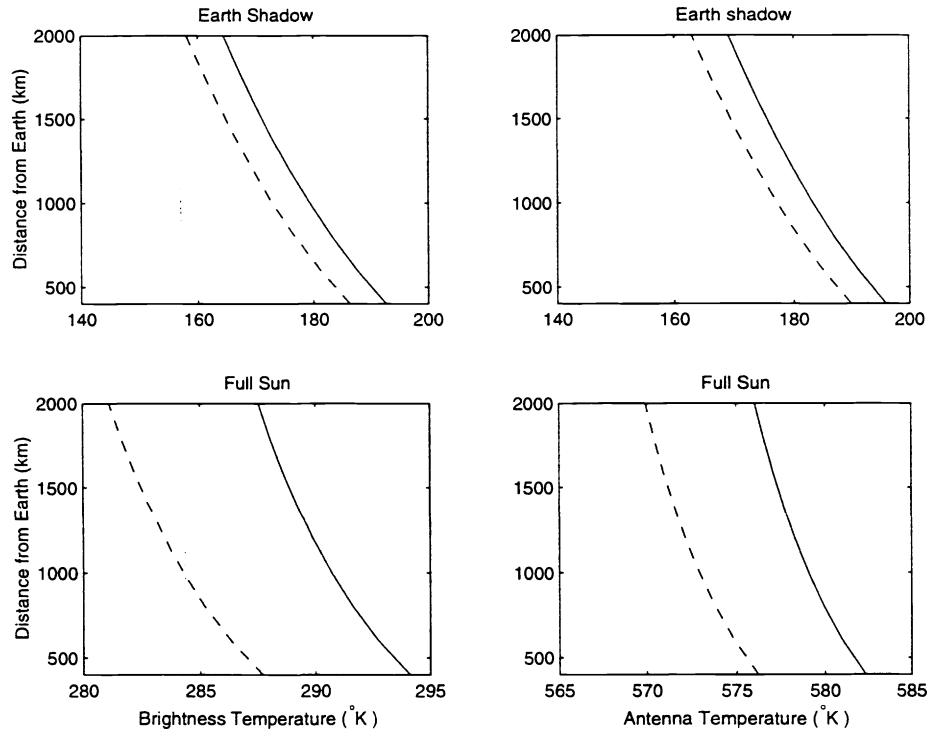

Figure 4. Antenna and brightness temperatures for different satellite orbit heights. Dashed line shows 300 GHz values, solid line shows 30 GHz values.

The range of temperatures fall well inside the temperatures of the Earth, Sun and cosmic background, thus detection of a satellite will be reliable for even low radiometric sensitivities and since absolute measurements of the temperatures are not sought the absolute accuracy is of little relevance. Some cases may not be as straightforward though, such as if a possibly colliding satellite is coming from a direction aligned with the Earth or Sun directions. In this case the main beam of the detector will be washed out at these temperature levels.

6. CONCLUSIONS

The radiometric temperatures of nanosatellties in the orbiting environment have been explored. The use of a radiometric collision avoidance sensor to allow safe passage through the orbit for nanosatellites has been discussed. The radiometric temperatures of the nanosatellites at various orbit heights lie well below the temperatures of the nearest radiation sources, the Earth and the Sun, and well above the cosmic background level. The scan size and beamwidths of the individual beams from the lens system could be decreased to allow more precise detection of satellites in Earth and Sun paths, since a great temperature contrast would be yielded. Yet, this will decrease the ability of detection over a wider field of view. This can be overcome by using more beams, but this will increase the size of the antenna array and therefore the entire system and introduce spill-over losses. Many trade-offs exist in the design where losses, size, weight and reliability are important factors.

Some open questions remain: (1) the transition from shadow to full sunlight is not immediate as assumed here, what effect does this have on the heating and cooling of the satellites? (2) how do the satellites heat and how could they reliably detect if they are spinning? (3) are the temperature contrasts great enough to implement insect vision algorithms? (4) are drastic collision avoiding manoeuvres safely possible for such small satellites in cluster environments? (5) indeed should these clusters detect and avoid as a cluster to avoid break-up? More intensive investigations can be carried out in the future if this type of technology is indeed required for nanosatellite clusters. In conclusion it appears that a fully integrated radiometric motion sensors may be a feasible instrument for collision avoidance for nanosatellites in Earth orbits.

ACKNOWLEDGMENTS

This work has been kindly funded by the Australian Research Council (ARC), and the Sir Ross & Sir Keith Smith Fund. The antenna front-end design is being designed in collaboration with A. J. Parfitt, CSIRO, NSW.

REFERENCES

1. S. Müncheberg, M. Krischke, and N. Lemke, "Nanosatellites and microsystems technology – capabilities, limitations and applications," *Acta Astronautica* **39**(9-12), pp. 799–808, 1996.
2. D. Goodfellow, G. Harmer, and D. Abbott, "mm-wave collision avoidance sensors: future directions," *Proc. SPIE Sensing and Controls with Intelligent Transportation Systems* **3525**, pp. 352–362, (Boston, USA), 1-5 Nov 1998.
3. N. Skou, *Microwave radiometer Systems: design and analysis*, Artech House Inc., USA, 1989.
4. J. R. Stuart and J. G. Stuart, "Revolutionary next generation satellite communications architectures and systems," *1997 IEEE Aerospace Conference. Proceedings* **3**, pp. 535–545, 1997.
5. A. Hansson, "From microsystems to nanosystems," *J. British Interplanetary Society* **51**, pp. 123–126, 1998.
6. J. R. Stuart, R. R. Coffey, and J. G. Stuart, "Economics of the new smaller and shorter lifetime geostationary communications satellites," *Pacific Telecommunications Council Fifteenth Annual Conference* **2**, pp. 531–536, 1993.
7. T. J. Jackson and T. J. Schmugge, "Algorithm for the passive remote sensing of soil moisture," in *Microwave Radiomet. Remote Sens. Appl.*, P. Pampaloni, ed., pp. 3–17, 1989.
8. J. C.-C. Shiue and L. R. Dod, "Remote sensing and microwave radiometry," in *Antenna Handbook; theory, applications and design*, Y. T. Lo and S. W. Lee, eds., ch. 22, pp. 1–51, Van Nostrand Reinhold Company Inc., USA, 1988.
9. L. Tsang, J. A. Kong, and R. T. Shin, *Theory of Microwave Remote Sensing*, John Wiley & Sons Inc., USA, 1985.
10. F. T. Ulaby, R. K. Moore, and A. K. Fung, *Microwave Remote Sensing: active and passive, Vol. 1: Microwave remote sensing fundamentals and radiometry*, Addison–Wesley Publishing Company, USA, 1981.

11. K. J. Button and J. C. Wiltse, eds., *Infrared and Millimeter Waves, Vol. 4: Millimeter Systems*, Academic Press Inc., USA, 1981.
12. D. Abbott and A. Parfitt, "Extension of the insect vision paradigm to millimeter waves," *Proc. SPIE* **3207**, pp. 103–106, (Pittsburgh, PA), Oct. 1997.
13. W. Rotman and R. F. Turner, "Wide-angle microwave lens for line source applications," *IEEE Trans. Antennas Propagat.* **AP-11**, pp. 623–632, Nov. 1963.
14. D. R. Gagnon, "Procedure for correct refocusing of the rotman lens according to snell's law," *IEEE Trans. Antennas Propagat.* **AP-37**, pp. 390–392, Mar. 1989.
15. D. M. Pozar, "Considerations for millimetre–wavelength printed antennas," *IEEE Trans. Antennas Propagat.* **AP-31**, pp. 740–747, Sept. 1983.
16. M. S. Smith, "Multiple beam crossovers for a lens-fed antenna array," *J. IERE* **55**, pp. 33–36, Jan. 1985.
17. E. O. Rausch, A. F. Peterson, and W. Wiebach, "Millimeter wave rotman lens," *Proc. 1997 IEEE National Radar Conf.* , pp. 78–81, (Syracuse, NY, USA), May 1997.
18. J. Kraus, *Radio Astronomy*, McGraw Hill Inc., USA, 1966.
19. J. M. Wallace and P. V. Hobbs, *Atmospheric Science: an introductory survey*, Academic Press Inc., USA, 1977.
20. D. C. Goodfellow and D. Abbott, "Collision avoidance for nanosatellite clusters using millimetre-wave radiometric motion sensors," To be presented at *Microelectronics and MEMs Symposium* **3891**, (Gold Coast, Australia), 27-29 Oct 1999.
21. C. Kittel and H. Kroemer, *Thermal Physics, 2nd Edition*, W. H. Freeman and Co., USA, 1980.
22. J. M. Uson and D. T. Wilkinson, "The microwave background radiation," in *Galactic and Extragalactic radio astronomy, 2nd Edition*, G. L. Verschuur and K. I. Kellermann, eds., ch. 14, pp. 606–607, Springer-Verlag New York Inc., USA, 1988.